poXNOR Morphological Transform based Feature Extraction for Mobile Robot Applications

Manigandan Nagarajan Santhanakrishnan, John Bosco Balaguru Rayappan, Ramkumar Kannan

Department of EIE, School of Electrical & Electronics Engineering, SASTRA University, Thanjavur – 613 401, Tamil Nadu, India (Tel: +91 4362 264101- Extn: 3642, 2255, 2165; e-mail: {manigandanns, ramkumar}@eie.sastra.edu, rjbosco@ece.sastra.edu).

Abstract: Efficient feature extraction algorithms are needed for localization, navigation of the autonomous mobile robot and fast mapping of the environment. This paper presents an experimental implementation of the morphological transform to extract the features of the environment. A novel percentage occupancy XNOR (poXNOR) approach has been proposed to address the same. To enhance the computational speed, compressed images of different sizes were generated using the laser range finder (LRF) data. Structure elements proportional to this image size were used for performing the poXNOR based morphological transformation. A significant 70% positive hit of the features with ±0.05 m accuracy was observed.

Keywords: Feature Extraction, Morphological Transform, Localization, Mobile Robots, Laser Range Finder, Transparent Obstacle

1. INTRODUCTION

Mobile robot navigation, localization and mapping have become a thrust area of research in the recent past. The successful implementation of the same lies in effective identification of stable features or permanent landmarks in the environment. Model based state estimation has uncertainties in localization of the mobile robot, which results in inaccurate navigation and mapping. This is primarily because of the approximations introduced in the mathematical models of the system, which leads to divergence of the state parameters from its true state. The problem of estimating the true states amidst noisy data is solved through various techniques including Kalman filter (KF), extended Kalman filter (EKF), unscented Kalman filter (UKF) or particle filter (PF) (Chatterjee et al., 2011; Holmes et al., 2009; Gustafsson et al., 2002) based correction. However the effectiveness of the above algorithms lies on the external vision sensors attached with the mobile robots and feature extraction algorithms (Ramkumar and Manigandan, 2012; Choi et al., 2008). These sensors and algorithms estimate the external world and aid in correcting the estimated states through the system models.

The dead reckoning sensor like wheel encoders is highly unreliable when it comes to exploration in an unknown and multi terrain environments. If the ground is slippery, data from the wheel encoders do not account for such deviations. This error is additive and so it accumulates over a period of time. At one point, the robot completely loses track and in literature this is referred as kidnapping problem (Andras et al., 2010). In order to correct the accumulated error, the concept of sensor fusion has evolved as one of the best solutions. Algorithms based on laser range finder (LRF) data for spatial information of the scene and the signatures extracted from visual device like camera were fused to get the best estimate of the mobile robot current location (Ho and Newman, 2006). Authors have highlighted the primary role of feature extraction techniques while implementing localization, navigation or target tracking algorithms (Ilas et al., 2011).

Loop closing is also an issue in mobile robots where the robot should identify the previously visited environment. This can be achieved by effective feature extraction algorithms, which is mainly determined by the various sensors employed in the robot. Basic vision sensors used for studying the environment are LRF, camera and sonar. Effectiveness of the signatures collected from camera depends on the light ambience and speed of the vehicle. The application of LRF in mobile robots is very significant for the fact that it can work with good precision and under low ambience as well.

The effectiveness of the feature extraction algorithm is decided by the place of location of the LRF. More than one LRF can be used at different levels to distinguish between the static and dynamic environments (Mastrogiovanni et al., 2012). But usage of more number of LRF decreases the energy efficiency of the system as a whole. The feature extraction can be done in polar space itself using geometric invariance technique (Noyer et al., 2010) but when implementing Kalman filter this has to be converted to Cartesian space for effective processing. Hough transform is applied to extract line features from the image generated by translating the LRF data to a 2D plane (Ogaz et al., 2009). Though it is an efficient method, computational time is a major limitation. Placement of artificial features to improve the performance of localization and mapping (Beinhofer et al., 2013) has been reported. But its restriction on the environment is yet to be addressed.

The appropriate detection of static or dynamic features and free space not only helps in effective localization but also enables the robot to navigate in the environment without

collision (Vatcha and Xiao, 2014; Wurm et al., 2010; Teslic et al., 2010; Se et al., 2001). Detection techniques for extremes, corners and discontinuities have also been elaborately discussed after LRF data pre-processing using a moving average filter (Duchon et al., 2012). A detailed comparison of various line fitting algorithms in terms of computational time and variance is also carried out (Nguyen et al., 2005).

Various morphological transformation techniques have been proposed to extract features from images and one such technique is hit-or-miss transform (Parape et al., 2012; Murray and Marshall, 2011). However the basic demerit of this method is that the structure elements have to be chosen exactly in coherence with the objects or the features to be hit. To overcome this restriction, percentage occupancy based hit-or-miss transform was proposed which can hit any feature with some allowable tolerance (Murray et al., 2009). This tolerance or deviation can be suitably selected by the user. Basically the hit-or-miss transform involves lot of mathematical manipulations and hence imposes computational burden when online processing and decision making is crucial.

Hence, in this work, a novel morphological transform using percentage occupancy XNOR (poXNOR) logic has been proposed. Wherein, only orthogonal features were considered for the experiment and the entire environment was set up only with orthogonal features. The data from the LRF is transformed to a 2D image plane for further processing. The data transferred from LRF to the image is considered the foreground and the rest of the area is background. In this technique, the back- and fore-ground match is separately considered. Taking them separately facilitates the normalization of the back ground scene. This occupies most of the image area compared to the feature, which is the fore ground information. Thus poXNOR method considerably reduces the computational burden and can be used on compressed images. Hence the existing limitations of online feature extraction and decision making can be resolved. Furthermore, the effectiveness of the proposed poXNOR technique was also tested when the autonomous mobile robot encounters transparent glass obstacles.

2. METHODLOGY

2.1 poXNOR Feature Extraction

The natural processing of images by human being for feature extraction is purely relative to the application. When it comes to the localization, mapping and navigation, humans do not use a very high resolution images. They try to extract the features of interest through search and match pattern. Various feature patterns of the environment are stored as markers in memory (brain). When a new environment is scanned by the eye, the brain tries to search for these markers available in memory from the developed image, which is relatively in compressed form (Pi et al., 2008). This compressed form of the image ensures fast processing to extract the relevant features. Most of the total processing time is shared by the decision making process. That is human beings are able to take quick and correct decisions most of the time even with a low resolution images or with lesser number of data. Therefore, the proposed technique tries to exploit the same dynamic activity of the human system. In this approach, the data from LRF is transformed to a 2D image which then is compressed suitably for further processing. Morphological transform based on the proposed poXNOR technique is applied to detect corner features from the developed 2D image. The methodology of the proposed model is shown in Fig. 1, which comprises of data acquisition, pre-processing, image compressions and morphological transform modules.

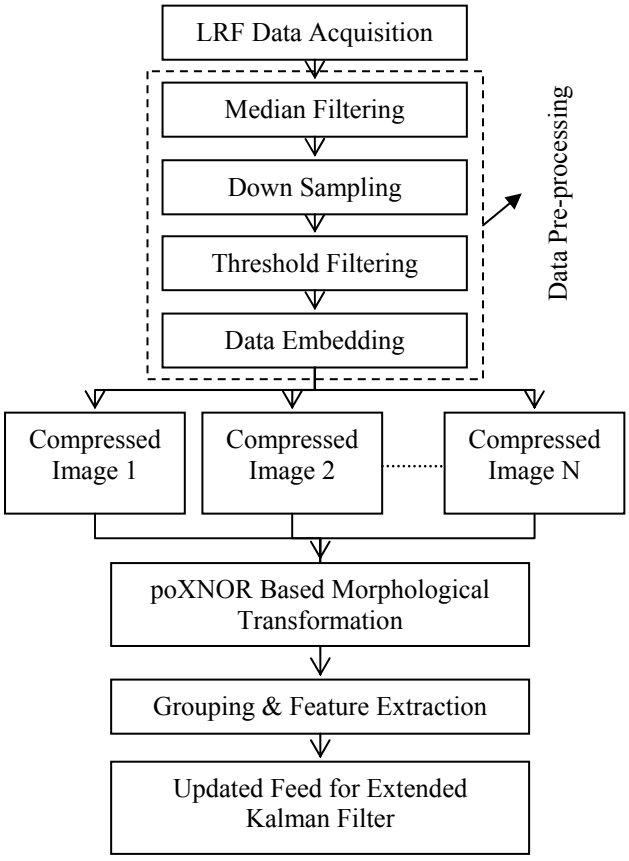

Fig. 1. Percentage occupancy XNOR (poXNOR) technique.

2.2 Experimental Setup & Data Pre-processing

Hokuyo URG-04LX-UG01 LRF is mounted on a four wheeled mobile robot, which under goes a random walk in the created environment shown in Fig. 2.

The environment was designed only with straight and corner features and care was taken that minimum of 2 features are visible at any point of time. The resolution of the LRF is 0.02 m and it can measure a maximum distance of 5.6 m. The scan angle is 240° with a step change of 0.35°. The operating region was restricted to 0.6 to 4 m for better performance. The robot was made to run at a speed of 0.25 m/sec.

The acquired raw data in the form of polar coordinates from LRF are processed through median filters for removing spurious noise and retain sharp edges. A sample of the scanned data by LRF before and after median filtering is shown in Fig. 3. The Fig. 3a shows the plot of raw data acquired from LRF. It is observed that there are lot of short

time spikes. These spikes fall in the high frequency range and have to be removed or otherwise it may lead to instability during localization of the mobile robot.

Fig. 2. Mobile robot with LRF in the created environment.

Median filtering technique was applied to remove these spikes or spurious points. The length of the window 'N' selected for median filtering is done based upon the noise level in the signal. The effect of length of the window on the signal is shown in Fig. 3b. If the length of the window is increased the high frequency noise gets attenuated substantially. But an optimum length has to be chosen because increase in length of the window increases the manipulation time. In the present case, the noise segment occupies approximately 7 sample points and so minimum of N=10 points are chosen as the length for median filter.

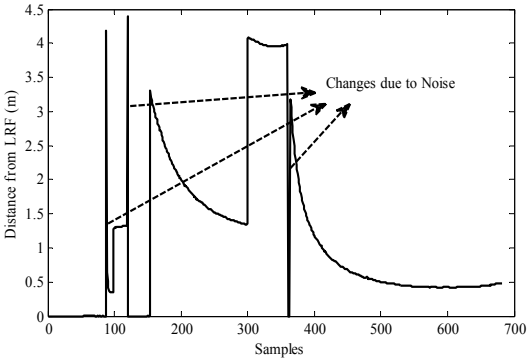

(a)

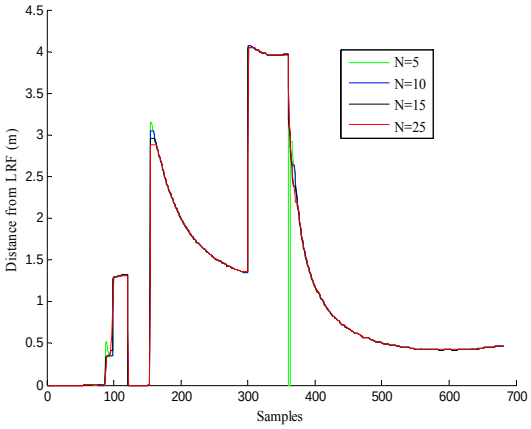

(b)

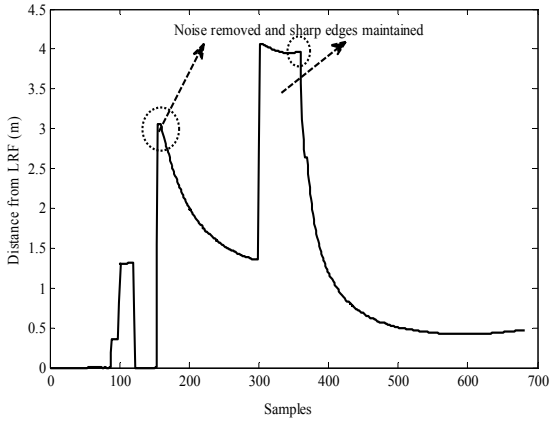

(c)

Fig. 3. a) Scanned data before median filtering, b) effect of length of window 'N' by median filtering on Fig 3a and c) scanned data after median filtering with N=10.

It is seen from Fig. 3c that the spurious points or spikes generated because of the light reflected from dusts particles and false edges are removed and the sharp edges are still maintained. These sharp edges can be the intersection points of any two straight line features such as walls which is considered as the major feature in this experiment. The processed signal is then converted to rectangular coordinates using (1).

$$\left.\begin{aligned} x &= r \times \cos(\theta) \\ y &= r \times \sin(\theta) \end{aligned}\right\} \tag{1}$$

where, θ varies from 30° to 210° in steps of 0.35° and r is the length of a point on the obstacle assumed in the created environment for each step angle.

Moreover, the obstacles in a real time environment can also be a transparent medium or in specific a glass material. Thus a method was devised to identify the presence of glass obstacle using LRF and the experimental setup for the same is shown in Fig 4.

Fig. 4. Experimental setup for transparent glass obstacle detection.

When laser light incidents on the glass obstacle or partition placed in front of a nontransparent wall, an interference pattern is formed between the light reflected from the front surface of the glass and the reflective nontransparent wall (Park et al., 2014; Sastikumar at al., 2010). This interference

pattern makes the nontransparent wall appear closer to the robot than its actual position. When the angle of incidence of laser moved towards the normal of the glass plane, the wall appeared to be further closer to the robot thus generating a parabolic pattern. This pattern was symmetrical with respect to the normal of the glass plane with its apex lying exactly on the glass plane itself as shown in Fig 5. This observation signifies the presence of a transparent glass partition in front of the mobile robot and its position.

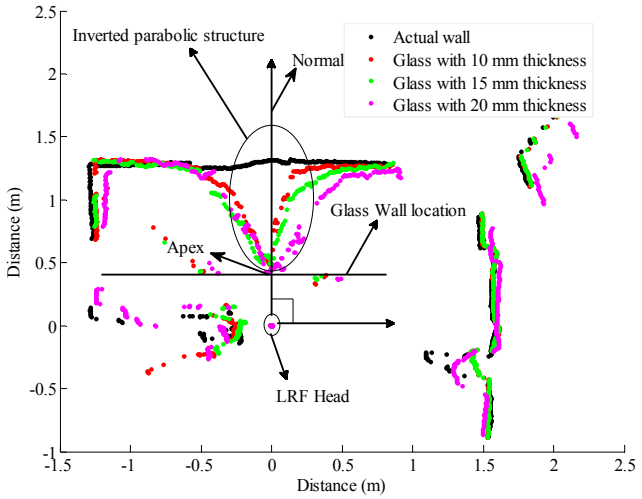

Fig. 5. Reflection pattern of laser beam for different angle of incidence and transparent glass obstacle thickness.

As the robot moves along the glass partition, this parabolic pattern keeps shifting in pace with the robot thus indicating the presence of a glass partition and its length. The parabolic pattern was consistent with respect to different thickness of the glass obstacle as shown in Fig 5 and hence chosen as the structure element. Direct morphological transform was applied to identify the presence of glass partition and its position using the parabolic structure element.

The plot of LRF data before and after filtering in 2D space is depicted in Fig. 6.

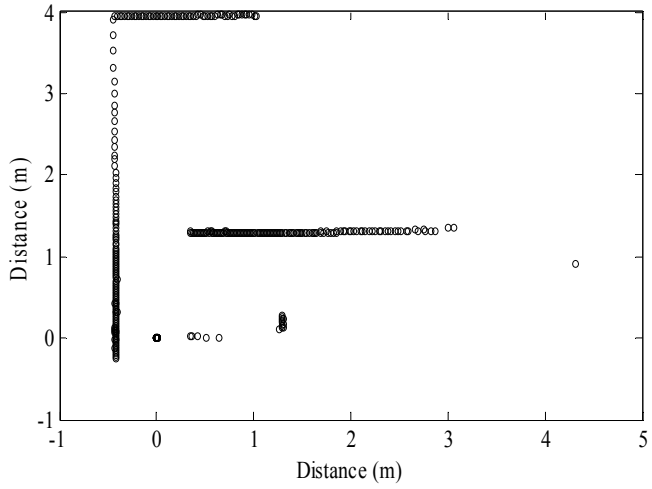

(a)

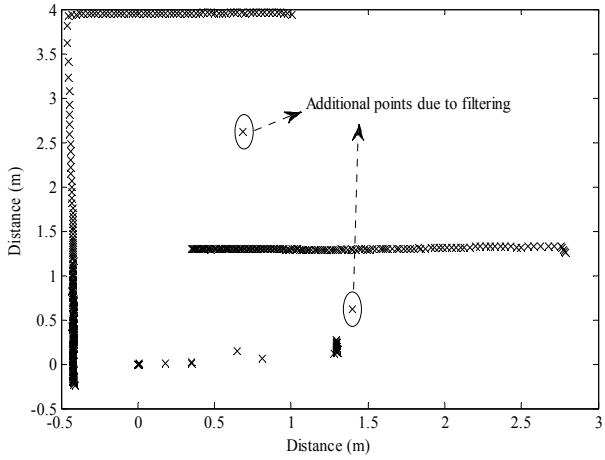

(b)

Fig. 6. a) 2D plot before and b) after median filtering.

Researchers have also used moving average filter (2) for removing these high frequency noises. The major advantage of using a moving average filter is that the various curved features can be easily extracted from noisy data. The effectiveness of it lies in proper selection of length of the window. Longer windows are required to remove high frequency noise, which will increase the computational time. Longer window length will smoother the entire signal and also introduces a spatial shift in the data points due to the delay introduced by the filter as shown in Fig. 7. Moreover, the LRF is largely discontinuous and hence is not continuously differentiable spatially leading to further spatial shift. For localization applications sharp edges are very crucial and any shift in the data points spatially affects the performance of the system as a whole. So, median filter was preferred over moving average filter in this experiment.

$$y(i)=\frac{1}{2M+1}\sum_{k=i-M}^{i+M}x(i+k) \tag{2}$$

Where, N=2M+1 the length of window

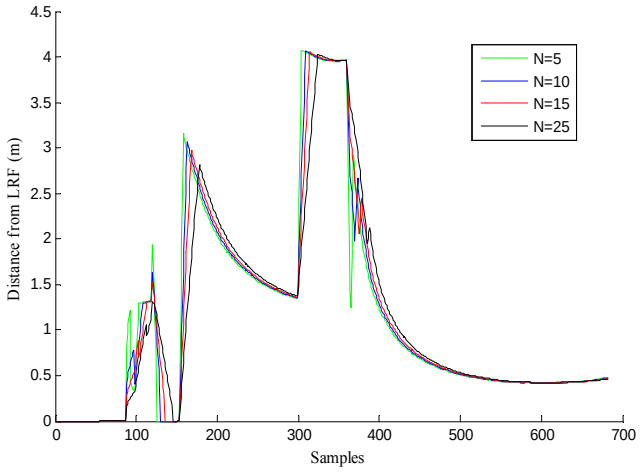

Fig. 7. Effect of length of window 'N' by moving average filtering.

Features of the objects of interest that are closer and orthogonal to the robot have large number of samples but the distant objects have few. So after filtering, the data is down sampled to remove grouping of data. This reduces the computational time and also removes the additional points that get introduced due to median filtering (Fig. 6b). This is done by imposing a threshold (T_d) on the Euclidean distance (E_d) between two consecutive points on the map using (3), where (x_p, y_p) are various points on the map. If $E_d < T_d$ then the points are retained or otherwise removed. The 2D map after down sampling is shown in Fig. 8.

$$E_d = \sqrt{(x_{p1} - x_{p2})^2 + (y_{p1} - y_{p2})^2} \tag{3}$$

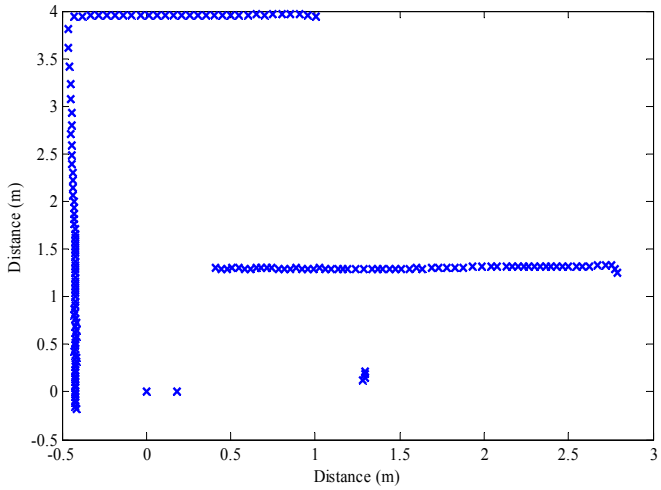

Fig. 8. 2D plot after down sampling.

Data embedding is done for even distribution of samples which increases the probability of line fitting and feature extraction. The distance between two samples in this data set (S) is kept at 3 cm after data embedding process. Morphological transform is performed on this data for feature extraction which is explained in detail in the following section.

2.3 Morphological Transform and Feature Extraction

A binary image (I_B) is generated through linear transformation of the data set S using (4). White pixel in the image represents the presence of a data point which is considered as the foreground.

$$\left.\begin{aligned} slopex &= \frac{1}{(X_{max} - X_{min})} \\ slopey &= \frac{1}{(Y_{max} - Y_{min})} \\ X_T &= I_s \times (x_i - X_{min}) \times slopex \\ Y_T &= I_s \times (y_i - Y_{min}) \times slopey \end{aligned}\right\} \tag{4}$$

where, (X_{max}, X_{min}, Y_{max}, Y_{min}) ϵ S

X_T, Y_T - The transformed pixel coordinates in the image
I_S - The chosen image size and i varies from 1 to Ns
Ns - The length of the set S

If X_T, Y_T is a fraction then it has to be rounded off to make sense in an image. A sample of the transformed image is shown in Fig. 9, which also highlights the absence of white pixel corresponding to the discontinuity in a major feature. Significantly, the proposed poXNOR method was able to detect this major feature even in the presence of a discontinuity. Also, the point features were created during transformation of minor features from the main LRF data. Noticeably, no separate filtering algorithms are required to remove these point features as the morphological transformation excludes them by virtue.

As the compression ratio (C_R) from (5) is increased more concrete information stays and minor features reflects as a point feature in the transformed image. The effectiveness of the morphological transformation lies in suitable selection of C_R which is generally a trade off between minor features and computational speed. The size of the structure element (S_e) is normalized with the maximum size I_S and S_e using (6). The maximum size of S_e and I_S are chosen based on the maximum distance fixed for the LRF. In this experiment max(I_S) and max(S_e) was chosen to be 125 x 125 and 17 x 17 respectively.

$$C_R = \frac{\max(I_s)}{I_s} \tag{5}$$

$$S_e = \frac{I_s \times \max(S_e)}{\max(I_s)} \tag{6}$$

where, $I_S \leq \max(I_S)$ and $S_e \leq \max(S_e)$. If S_e is a fraction then it is rounded off to make sense.

Structure elements of different orientations are created with various step angles (θ_S°) as shown in Fig. 10. Corners of 90° angle generated by perpendicular lines are chosen to be the feature for this experiment. If one wishes to chose any other angle a corresponding structure element can be generated and adopted.

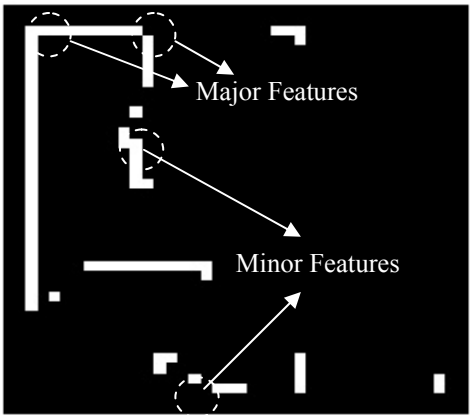

Fig. 9. Transformed image ($I_S = 35 \times 35$).

The structure element thus generated is moved on the image to identify any match. The advantage in this proposed method is that the location of the information (white pixel) is known apriori. So the structure element can be moved only along the white pixel region which significantly reduces the computational time. The normal morphological transforms searches for a pattern in the entire image, so the

computational time is comparatively very high. Two different approaches, 1. Exact XNOR (eXNOR) match and 2. The proposed poXNOR match are used and compared. The logical operation procedure is shown in (7).

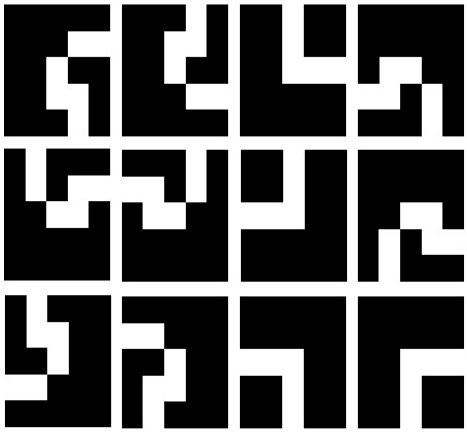

Fig. 10. Structure element with $\theta_S = 30°$.

$$eXNOR = I_R S_e + \overline{I_R}\,\overline{S_e} \tag{7a}$$

$$\left.\begin{aligned} w_1 &= \left|\left\{X_{ij} \mid X_{ij} = 1, X_{ij} \in I_R S_e\right\}\right| \\ w_2 &= \left|\left\{Y_{ij} \mid Y_{ij} = 1, Y_{ij} \in \overline{I_R}\,\overline{S_e}\right\}\right| \end{aligned}\right\} \tag{7b}$$

$$poXNOR = \frac{1}{2}\left(\frac{w_1}{N_W} + \frac{w_2}{N_B}\right) \tag{7c}$$

Equations 7a, 7b are purely logical operations and 7c is arithmetic. I_R is the resized image of I_B to match the size of S_e. *eXNOR*, w_1 and w_2 represents the number of white pixels in the resultant image. N_W and N_B represent the number of white and black pixels in w_1 and w_2 respectively.

poXNOR is a normalized value based on which the existence of a feature is decided. Morphological transform was performed on the image using (7) and the features are extracted. The eXNOR approach is completely logical it gives importance to both the fore ground and back ground information. So any small deviation of the compared sectional image from the structure element due to noise will result in non detection of the existing feature. Whereas the poXNOR method is partially logical and partially arithmetic and this gives the liberty of independent normalisation for the back ground and fore ground match. Moreover if due to restrictions if one is forced to have a larger image size then the structure element also proportionally increases in size. This results in the number of black pixels (back ground) to be much greater than the white pixels (fore ground). Under these circumstances also, the poXNOR method gives better results as the decision is taken based on the percentage occupancy. The results of the proposed technique are discussed in next section.

3. RESULTS AND DISCUSSION

In the transformed image the white pixels represents the fore ground and the black pixels the back ground. The w1 and w2 in (7) gives the fore ground and back ground match respectively. The eXNOR approach detects a feature only if the Se exactly matches the IR including the back ground. Whereas the poXNOR allows a percentage of tolerance on fore and back ground match. The experiment was performed for 3 different θS° of the structure element.

The results in terms of number of the feature hits for 80 continuous scans with different compression ratios are shown in Table 1. The total number of major features (TM) was 280 in 80 scans and this number includes repeated features as well. The percentage hits (PH) was calculated using (8).

$$P_H = \frac{T_H - E_H}{T_M} \times 100 \tag{8}$$

where, T_H is the total hits and E_H is the error in hits. It is evident from Table 1 that best results are achieved by maintaining the C_R at 3.6 and using poXNOR method. As the C_R is increased the P_H also increases till one point and any further increase in C_R the P_H becomes unbounded. This unbounded condition arises due to the fact that increase in C_R beyond a value creates more number of point features in the resized image. Moreover S_e also reduces with increase in C_R.

So there is more probability of identifying false features from the environment. Thus the total hits show a value much higher than the actual number of features that can be identified in the total 80 scans. So an optimum point needs to be fixed on the C_R and corresponding extracted features. The most optimum value of C_R and P_H from this experiment was found to be 3.6 and 70% on average respectively. On the other hand it is seen that the eXNOR method has an increase in trend on P_H always, were as the total hits is relatively less compared to poXNOR. The P_H of eXNOR is nearly 65% on average for C_R of 6.25 but the % Error in Hits has drastically increased to 23% on average which significantly reduces the belief factor on the extracted features. So it is evident that poXNOR method is best suited for morphological transform based feature extraction. The retranslated feature coordinates extracted through poXNOR based morphological transform is shown in Fig. 11.

The resizing of image is done linearly on X axis and Y axis equally and along one direction only. So the quantization error introduced because of this compression can be easily quantified and corrected during retranslation. The error on the retranslated coordinates on the XY map was found to be less than 0.05m.

These extracted features are used for state and covariance updating in EKF using (9).

$$\left.\begin{aligned} \hat{X}_{k+1}^{-} &= f\left(\hat{X}_k^{+}, U_k, \omega_k\right) \\ \hat{Z}_k &= h(\hat{X}_{k+1}^{-}, \vartheta_k) \\ P_{k+1}^{-} &= A_k P_k^{+} A_k^T + \omega_k Q_k \omega_k^T \\ K_k &= P_{k+1}^{-} H_k^T \left(H_k P_{k+1}^{-} H_k^T + \vartheta_k R \vartheta_k^T\right)^{-1} \\ \hat{X}_{k+1}^{+} &= \hat{X}_{k+1}^{-} + K_k\left(Z_{k+1} - h(\hat{X}_{k+1}^{-}, \vartheta_k)\right) \\ P_{k+1}^{+} &= \left(I - K_k H_k\right) P_{k+1}^{-} \end{aligned}\right\} \tag{9}$$

Table 1. Comparison of feature hits for different C_R and $\theta_S°$
(Total scan was 80 and total physically identified features were 280)

Compression Ratio (C_R)	Step Angle ($\theta_S°$)	poXNOR Hits		eXNOR Hits		% Hits (P_H)	
		Total Hits (T_H)	% Error in Hits	Total Hits (T_H)	% Error in Hits	poXNOR	eXNOR
1	10	7	0	0	0	2.5	0
	30	8	0	0	0	3	0
	45	7	0	0	0	2.5	0
1.67	10	67	6	36	0	23	13
	30	55	7	36	0	18.5	13
	45	53	8	36	0	17.5	13
2.1	10	118	7	53	0	39.5	19
	30	96	7	52	0	32	18.5
	45	91	8	52	0	30	18.5
3.6	10	221	8	134	0	73	48
	30	208	8	135	0	70	48
	45	198	6	132	0	67	47
6.25	10	628	68	242	22	Deviation is more	67.5
	30	602	66.5	238	21		67
	45	628	68.5	233	27		61

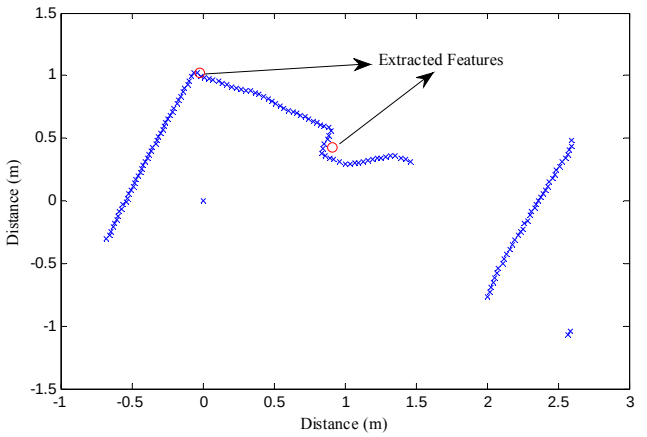

(a)

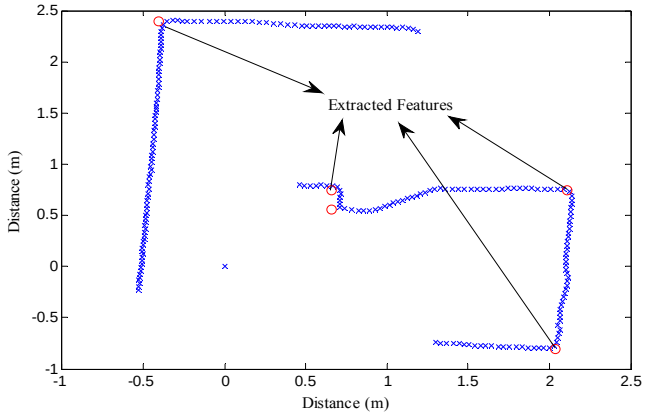

(b)

Fig. 11. The retranslated feature coordinates on the XY plane.

Where, k is the sample time instant, U_k the input, ω_k the system model noise, A_k the Jacobian of the system model $f(.)$, H_k the Jacobian of the measurement model $h(.)$, ϑ_k the measurement model noise, Q_k the process noise covariance, R_k the measurement noise covariance, P_k the covariance, K_k the Kalman gain and Z_k the actual measurement from the sensor. The feature coordinates extracted using poXNOR method is fed to Z_k in (9) for further updating. If the variance on Z_k is large then the convergence of P_k gets affected which results in inaccurate correction of the estimated state. Since this is a closed loop process, the corrected states goes unbounded over a period of time resulting in instability of the entire system.

The advantage of this method lies in the reduced and effective processing time and increased feature identification. This obviously will enhance the navigation speed of the mobile robot in the environment. The limitation of the study however lies in adaptive selection of C_R and θ_S. The environment used for this study was highly restricted with orthogonal, static and known features.

4. CONCLUSIONS AND FUTURE PERSPECTIVE

Images of various sizes were generated using the rectangular coordinates derived from the LRF data. The poXNOR based morphological transform was performed using a structure element of different size and orientations. The results were compared with the eXNOR approach. The poXNOR was found to be better in terms of P_H on the features. It was found that poXNOR method gave 70% positive hits on feature when compared with eXNOR which gave only 48%. Since the processing is done on a reduced size of an image, the

processing time also improved when compared to the normal line fitting approaches. This advantage can be utilized in effective and fast navigation of the mobile robot. As a special case, an optical interference based technique was used to detect the position of glass obstacles using LRF. The selection of C_R and θ_S can be made adaptive through any learning and decision making algorithm for robust performance of the mobile robot in dynamic and unknown environment. These works are proposed for further study.

ACKNOWLEDGEMENT

The authors wish to express their sincere thanks to the Defense Research and Development Organisation (CAIR-DRDO), New Delhi, India for their financial support (Project ID: ERIP-ER-0903808 dt 23.4.10). They also wish to acknowledge SASTRA University, Thanjavur for extending financial & infrastructural support (Project ID: R&M0024/SEEE-008/2012-2013) to carry out this work.

REFERENCES

Andras, M., Mircea, P., Levente, T., Istvan, S., and Gheorghe, L. (2010). A new approach in solving the kidnapped robot problem. *41st Int. Symp. Robotics (ISR) and 6th Int. Conf. Robotics (ROBOTIK), IEEE*, 7-9 Jun, pp. 1-6.

Beinhofer, M., Muller, J., and Burgard, W. (2013). Effective landmark placement for accurate and reliable mobile robot navigation, *Robotics and Autonomous Systems, Elsevier,* Vol. 61(10), pp. 1060-1069. DOI:10.1016/j.robot.2012.08.009

Chatterjee, A., Ray, O., Chatterjee, A., and Rakshit, A. (2011). Development of a real-life ekf based slam system for mobile robots employing vision sensing. *Expert Systems with Applications, Elsevier,* Vol. 38, pp. 8266-8274. DOI: 10.1016/j.eswa.2011.01.007

Choi, Y. H., · Lee, T. K., and · Oh, S. Y. (2008). A line feature based slam with low grade range sensors using geometric constraints and active exploration for mobile robot. *Autonomous Robots, Springer,* Vol. 24(1), pp. 13-27. DOI: 10.1007/s10514-007-9050-y

Duchon, F., Dekan, M., Jurisica, L., and Vitko, A. (2012). Some applications of laser range finder in mobile robotics*, J. CEAI,* Vol. 14 (2), pp. 50-57.

Gustafsson, F., Gunnarsson, F., Bergman, N., Forssell, U., Jansson, J., Karlsson, R., and Nordlund, P. J. (2002). Particle filters for positioning, navigation and tracking. *IEEE Trans., Signal Processing,* Vol.50(2), pp. 425-437. DOI: 10.1109/78.978396

Ho, K. L. and Newman, P. (2006). Loop closure detection in slam by combining visual and spatial appearance. *Robotics and Autonomous Systems, Elsevier*, Vol. 54, pp. 740-749. DOI: 10.1016/j.robot.2006.04.016

Holmes, S. A., Klein, G., and Murray, D. W. (2009). An $O(N^2)$ square root unscented Kalman filter for visual simultaneous localization and mapping. *IEEE Trans., Pattern Analysis and Machine Intelligence*, Vol. 31(7), pp. 1251-1263. DOI: 10.1109/TPAMI.2008.189.

Ilas, C., Novischi, D., Paturca, S., and Ilas, M. (2011). Real-time image processing algorithms for object and distances identification in mobile robot trajectory planning. *J. CEAI,* Vol. 13(2), pp. 32-37.

Mastrogiovanni, F., Sgorbissa, A., and Zaccaria, R. (2012). How the location of the range sensor affects EKF-based localization. *J. Intell. Robot Syst., Springer,* Vol. 68, pp. 121-145. DOI: 10.1007/s10846-012-9673-x

Murray, P. and Marshall, S. (2011). A new design tool for feature extraction in noisy images based on gray scale hit-or-miss transforms. *IEEE Trans., Image Process*., Vol. 20(7), pp. 1938-1948. DOI: 10.1109/TIP.2010.2103952

Murray, P., Marshall, S., and Bullinger, E. (2009). The percentage occupancy hit or miss transform. *17th European Signal Processing Conference (EUSIPCO 2009)*, Glasgow, Scotland, August 24-28, pp. 253-257.

Nguyen, V., Martinelli, A., Tomatis, N., and Siegwart, R. (2005). A comparison of line extraction algorithms using 2D laser range finder for indoor mobile robotics. *Int. Conf. On Intelligent Robots and Systems, IEEE,* August 2-6, pp. 1929-1934. DOI: 10.1109/IROS.2005.1545234

Noyer, J. C., Lherbier, R., and Fortin, B. (2010). Automatic feature extraction in laser range finder data using geometric invariance. *44th Int. Conf. Signals, Systems and Computers (ASILOMAR), IEEE*, 7-10 Nov, pp. 199-203. DOI: 10.1109/ACSSC.2010.5757498

Ogaz, M., Sandoval, R., and Chacon, M. (2009). Data processing from a laser range finder sensor for the construction of geometric maps of an indoor environment. *52nd Int. Midwest Symp., Circuits and Systems (MWSCAS), IEEE*, 2-5 Aug, pp. 306-313. DOI: 10.1109/MWSCAS.2009.5236093

Parape, C. D. K., Premachandra, H. C. N., Tamura, M., and Sugiura, M. (2012). Morphological hit-or-miss transform based approach for building damage estimation from VHR airborne imagery in 2011 Pacific coast of Tohoku earthquake and tsunami. *Conf. Proc. International Archives of the Photogrammetry, Remote Sensing and Spatial Information Sciences*, Melbourne, Australia, 25 Aug-01 Sep, Vol. 39-B3, pp. 509-512. DOI: 10.5194/isprsarchives-XXXIX-B3-509-2012

Park, J., Matson, E. T., and Jung, J. W. (2014). A Method to Localize Transparent Glass Obstacle using Laser Range Finder in Mobile Robot Indoor Navigation. In Kim, J. H., Matson, E.T., Myung, H., Xu, P., and Karry. F., *Robot Intelligence Technology and Applications 2, Advances in Intelligent Systems and Computing 274*, 29-35. Springer, Switzerland. DOI: 10.1007/978-3-319-05582-4_3

Pi, Y., Liao, W., Liu, M., and Lu, J. (2008). *Pattern recognition techniques, technology and applications*. Chapter 17, Theory of Cognitive Pattern Recognition, Peng-Yeng Yin (Ed.), InTech.

DOI: 10.5772/90

Ramkumar, K. and Manigandan, N. S. (2012). Stochastic filters for mobile robot SLAM problems - A review. *Sensors & Transducer Journal, IFSA,* Vol. 138(3), pp. 141-149.

Sastikumar, D., Gobi, G., and Renganathan, B. (2010). Determination of the thickness of a transparent plate using a reflective fiber optic displacement sensor. *Optics and Laser Technology, Elsevier*, vol. 42(6), pp. 911-917.
DOI:10.1016/j.optlastec.2010.01.008

Se, S., Lowe, D., and Little, J. (2001). Vision-based mobile robot localization and mapping using scale-invariant features. *Robotics and Automation, IEEE Proc. Int. Conf. ICRA*, Vol.2, pp. 2051-2058.
DOI: 10.1109/ROBOT.2001.932909

Teslic, L., Skrjanc, I., and Klancar, G. (2010). Using a lrf sensor in the Kalman filtering based localization of a mobile robot. *ISA Transactions,* Vol. 49(1), pp. 145-153.
DOI: 10.1016/j.isatra.2009.09.009

Vatcha, R. and· Xiao, J. (2014). Detection of robustly collision-free trajectories in unpredictable environments in real-time. *Autonomous Robots, Springer,* Vol. 37(1), pp. 81-96.
DOI: 10.1007/s10514-013-9377-5

Wurm, K. M., Stachniss, C., and Grisetti, G. (2010). Bridging the gap between feature and grid-based slam. *Robotics and Autonomous Systems, Elsevier,* Vol. 58(2), pp. 140-148.
DOI: 10.1016/j.robot.2009.09.009